

UC Irvine

UC Irvine Previously Published Works

Title

Delineating the role of MITF isoforms in pigmentation and tissue homeostasis.

Permalink

<https://escholarship.org/uc/item/9q79g9rr>

Journal

Pigment cell & melanoma research, 33(2)

ISSN

1755-1471

Authors

Flesher, Jessica L
Paterson-Coleman, Elyse K
Vasudeva, Priya
et al.

Publication Date

2020-03-01


DOI

10.1111/pcmr.12828

Peer reviewed

ORIGINAL ARTICLE

Delineating the role of *MITF* isoforms in pigmentation and tissue homeostasis

Jessica L. Flesher^{1,2} | Elyse K. Paterson-Coleman³ | Priya Vasudeva⁴ |
Rolando Ruiz-Vega^{2,5,6} | Michaela Marshall⁷ | Eric Pearlman⁷ | Grant R. MacGregor^{5,8} |
Jonathan Neumann⁸ | Anand K. Ganesan^{1,2,4} 

¹Department of Biological Chemistry, University of California, Irvine, CA, USA

²Center for Cancer Systems Biology, University of California, Irvine, CA, USA

³Environmental Health and Safety, Oregon Health and Science University, Portland, OR, USA

⁴Department of Dermatology, University of California, Irvine, CA, USA

⁵Department of Developmental and Cell Biology, University of California, Irvine, CA, USA

⁶Center for Complex Biological Systems, University of California, Irvine, CA, USA

⁷Department of Ophthalmology, University of California, Irvine, CA, USA

⁸Irvine Transgenic Mouse Facility, University Laboratory Animal Resources, Office of Research, University of California, Irvine, CA, USA

Correspondence

Anand K. Ganesan, Department of Dermatology and Biological Chemistry, 202 Sprague Hall, Irvine, CA 92697-2400, USA.
Email: aganesan@uci.edu

Funding information

National Center for Research Resources, Grant/Award Number: 1S10RR025496-01; NIH Office of the Director, Grant/Award Number: 1S10OD010794-01 and 1S10OD021718-01; National Institute of Arthritis and Musculoskeletal and Skin Diseases, Grant/Award Number: R01AR063116; Chao Family Comprehensive Cancer Center; National Cancer Institute, Grant/Award Number: P30CA062203, R01CA151513, T32CA009054-37 and U54-CA217378

Abstract

MITF, a gene that is mutated in familial melanoma and Waardenburg syndrome, encodes multiple isoforms expressed from alternative promoters that share common coding exons but have unique amino termini. It is not completely understood how these isoforms influence pigmentation in different tissues and how the expression of these independent isoforms of *MITF* is regulated. Here, we show that melanocytes express two isoforms of *MITF*, *MITF-A* and *MITF-M*. The expression of *MITF-A* is partially regulated by a newly identified retinoid enhancer element located upstream of the *MITF-A* promoter. *Mitf-A* knockout mice have only subtle changes in melanin accumulation in the hair and reduced *Tyr* expression in the eye. In contrast, *Mitf-M*-null mice have enlarged kidneys, lack neural crest-derived melanocytes in the skin, choroid, and iris stroma, yet maintain pigmentation within the retinal pigment epithelium and iris pigment epithelium of the eye. Taken together, these studies identify a critical role for *MITF-M* in melanocytes, a minor role for *MITF-A* in regulating pigmentation in the hair and *Tyr* expression in the eye, and a novel role for *MITF-M* in size control of the kidney.

KEYWORDS

alternative promoters, choroid, CRISPR/CAS9, isoforms, melanogenesis, microphthalmia-associated transcription factor, *MITF*, retinal pigment epithelium, retinoids

1 | INTRODUCTION

In the human genome, alternative promoters are present in 30%–50% of coding genes where they contribute to the diversity of the proteome and allow more sophisticated control of gene expression (Davuluri, Suzuki, Sugano, Plass, & Huang, 2008). Alternative promoters contain unique sequences to regulate the expression of distinct isoforms in response to environmental or developmental cues. Genes including *EIF1AX* and *HBG1* utilize alternative promoters where one promoter lacks a TATA box for the expression of isoforms at the correct time during development (Davis & Schultz, 2000; Davuluri et al., 2008). In differentiation, alternative promoters allow for the expression of isoforms in tissue and cell-specific manners (Landry, Mager, & Wilhelm, 2003). Aberrant use of alternative promoters is associated with cancer. Transcripts generated through the *TP53* P1 promoter produce p53 protein isoforms containing transactivation domains that allow p53 to regulate its tumor suppressor functions (Kim & An, 2016), while transcription from the P2 promoter produces p53 protein that lacks the transactivation domains (Kim & An, 2016), and promote breast cancer stem cell maintenance (Arsic et al., 2015).

Microphthalmia-associated transcription factor (MITF) is the master regulator of melanocyte cell identity, controlling the production of melanin that gives skin, hair, and eyes color (Vachtenheim & Ondrusov, 2013). Mutations in the human *MITF* locus are associated with increased risk for familial melanoma, Waardenburg syndrome, and Tietz syndrome (Bertolotto et al., 2011; Pingault et al., 2010). The *MITF* gene has nine distinct isoforms that are produced using alternative first coding exons (Bharti, Liu, Csermely, Bertuzzi, & Arnheiter, 2008). Some isoforms have ubiquitous expression, while others are more restricted to specific cell types and tissues (Amae et al., 1998). While the amino-terminus of MITF isoforms differ, all isoforms contain the basic helix–loop–helix leucine zipper that is required for DNA binding and dimer formation with other bHLH family transcription factors (Pogenberg et al., 2012). *Mitf* mutations in mice cause varied phenotypes with distinct features including premature graying, microphthalmia, and depigmentation (Levy, Khaled, & Fisher, 2006). Although mice with mutations in the promoter regions of *Mitf* have been identified (Steingrímsson, Copeland, & Jenkins, 2004), the mutant alleles involve the loss of multiple isoforms, so it is still unclear how specific isoforms of MITF regulate pigmentation. Established methods for studying the role of *Mitf* isoforms rely on (a) mutant alleles that affect multiple isoforms (Steingrímsson et al., 2004); (b) examination of the expression pattern of isoforms in target tissues of wild-type and *Mitf* mutant animals to infer their function during development (Bharti et al., 2008); (c) isoform-specific overexpression studies to determine the function of individual isoforms (Michael et al., 2018); or (d) isoform-specific knockouts as previously performed (Bharti et al., 2012; Phelep et al., 2017). More precise knockout models are needed to deconvolute the role of individual isoforms in tissue development and disease.

While published studies suggest that *MITF-M* is the main isoform expressed in melanocytes, the role of other *MITF* isoforms in

Significance

Mutations in *MITF* cause hypopigmentation and increase the risk for familial melanoma in humans. There are multiple different isoforms of *MITF*, and it is currently unclear how these different isoforms contribute to pigment cell development in the eye, hair, and skin. In this study, we identified two isoforms of *MITF* that are present in melanocytes of the skin and use genome editing technology to block the expression of one or the other of these isoforms in mice. Taken together, our work illustrates how protein isoforms can differentially contribute to biological phenotypes, findings that have relevance to human disease.

melanocyte biology has not been studied. Here, we demonstrate that the human *MITF-A* isoform is expressed in melanocytes and its expression is regulated by retinoids. To distinguish the roles of *Mitf-A* and *Mitf-M* in pigment cell development and melanogenesis, we use CRISPR/Cas9 to generate *Mitf-A* and *Mitf-M* isoform-specific knockout mice. We observe that *Mitf-A* knockout mice have a subtle loss of pigmentation in the hair, while *Mitf-M* knockout mice lack melanocytes in the epidermis, hair follicle, iris, and choroid. Our study illustrates the utility of a CRISPR/Cas9-based approach to define specific roles for MITF isoforms in tissue development and pigmentation.

2 | MATERIALS AND METHODS

2.1 | Mouse strains and genotyping

All animal experiments were approved by the UC Irvine Institutional Animal Care and Use Committee (IACUC) (AUP-17-230). *ROSA^{mTmG/mTmG}* mice (Stock No: 007576), C57BL/6J (Stock No: 000664), and B6(Cg)-Tyr^{c-2J}/J mice (Stock No: 000058) were obtained from The Jackson Laboratory. C57BL/6NTac zygotes for genome editing were obtained from Taconic Biosciences. C57BL/6N mice used for *crb1* genotyping were obtained from the KOMP repository. Genotyping primers for *Mitf* mice were designed following the characterization of deletions. All other genotyping primers follow guidelines provided by The Jackson Laboratory. Genotyping primers are provided in Table S5 and additionally described in Appendix S1.

2.2 | CRISPR/Cas9 genome editing

Mitf mutant mice were generated by pronuclear injection of CRISPR/Cas9 reagents into C57BL/6NTac zygotes. Guide RNAs (gRNAs) were designed using sgRNA Designer (Broad Institute, MIT) and GTScan (EMBL, Australia) algorithms. Guide-RNA templates were synthesized by PCR using oligos and GBLOCK oligos (IDT). In vitro-transcribed (IVT) gRNA was made using mMessage mMachine (Thermo Fisher) and purified by MEGAclear Kit (Thermo Fisher).

Cas9 mRNA was made by IVT using the same reagents with px330 plasmid (Addgene plasmid #42230) (Cong, Ran, Cox, Lin, & Barretto, 2013). RNAs were injected at 20 ng/μl each. Resulting mice were screened by PCR and T7 endonuclease. T7 endo-positive alleles were amplified by nested PCR and Sanger-sequenced. CRISPR alleles were separated from hemizygous founders by outcrossing the mice to C57BL/6J mice (The Jackson Laboratory, Stock No: 000664). Lines were established from the F2 generation that was predicted to knock out expression of each specific *Mitf* transcript. All primers and gRNA used are listed in Table S6.

The *Mitf*^{em1Gene} allele (MGI: 6273202) contains a 7 bp deletion in chromosome 6, spanning 97,807,194–97,807,200 in Ensembl assembly GRCm38.p6. The deletion in this allele results in a loss of the *Mitf-A* isoform, designated as *Mitf* variant 202 in Ensembl and NM_001113198 in NCBI. Homozygotes for the *Mitf*^{em1Gene} are referred to as *Mitf-A* knockouts or nulls. The *Mitf*^{em2Gene} allele (MGI: 6273203) contains an 18 bp deletion in chromosome 6, spanning 97,991,944–97,991,961 in Ensembl assembly GRCm38.p6. The deletion in the *Mitf*^{em2Gene} allele results in a loss of the *Mitf-M* isoform through the loss of a splice site, and this is designated as *Mitf* variant 201 in Ensembl and NM_008601 in NCBI. Homozygotes for the *Mitf*^{em2Gene} deletion are referred to as *Mitf-M* knockouts or nulls.

2.3 | Single-cell isolation, sorting, and RNA-seq

Shaved and depilated whole back skin of P54 *ROSA*^{mTmG} mice was dissociated into a single-cell suspension and incubated with Ghost Dye Red 780 (Tonbo Biosciences) to identify viable cells. Live GFP+ and tdTomato+ cells were sorted using a BD FACSAria Fusion Sorter, and RNA-seq was performed as described in Appendix S1. The data discussed in this publication have been deposited in NCBI's Gene Expression Omnibus (Edgar, Domrachev, & Lash, 2002) and are accessible through GEO Series accession number GSE138538 (<https://www.ncbi.nlm.nih.gov/geo/query/acc.cgi?acc=GSE138538>).

2.4 | Analysis of read junctions

BAM files generated in Tophat were visualized against the annotated mm10 transcriptome in IGV (version 2.4.8) (Robinson et al., 2011; Thorvaldsdóttir, Robinson, & Mesirov, 2013). After identifying read junctions present between exons 1A to 1B, 1B to 2A, and 1M to 2A, read junctions were counted between exons 1B and 2A as proxy for *Mitf-A* as no other isoforms containing exon 1B were found. Read junctions between exons 1M and 2A were counted as proxy for *Mitf-M*. The percentage of *Mitf-A* and *Mitf-M* transcripts was determined for GFP+ and tdTomato+ cells. To account for differential expression of *Mitf* between melanocytes and other skin cells, the percentage of each isoform was multiplied by the relative abundance of *Mitf* in the respective cell population. Pearson's chi-squared test performed in R (version 3.3.2) was used to determine whether the expression of individual isoforms was significantly different between samples.

Human RNA-seq raw data files (SRP039354) were retrieved from the SRA database (Haltaufderhyde & Oancea, 2014) and aligned to

the NCBI human reference genome GRCh38 using Tophat alignment software (version 2.0.12) (Trapnell, Pachter, & Salzberg, 2009). BAM files were visualized as described above. To delineate isoforms containing exon 1B, the proportion of read junctions from upstream exons (1A, 1J, 1C, 1E, and 1H) to 1B was multiplied by the proportion of read junctions to 2A containing 1B. Read junctions between 1M and 2A were still used as proxy for *MITF-M*.

2.5 | Melanocyte isolation using CD117 microbeads

Neonatal mouse melanocytes were collected as previously described (Godwin et al., 2014; Liggins et al., 2018). Mice less than 3 days old were euthanized and sterilized. Skin was removed and cleaned of muscle. The epidermis was separated from the dermis following a 1-hr incubation in 5mg/ml trypsin (Sigma-Aldrich) at 37°C. The epidermis was chopped in 0.25% trypsin-EDTA solution (Gibco) and resuspended in RPMI with 5% FBS. The resuspended cells were filtered using a 100-μm cell strainer followed by a 40-μm cell strainer. Cells were sedimented and washed in PBS (pH 7.2) with 0.5% BSA (Fisher Scientific). The cell pellet was resuspended and incubated with CD117 MicroBeads (Miltenyi Biotec) following the manufacturers' protocol. CD117-positive and CD117-negative cells were then lysed for RNA extraction using RNAeasy Mini Kit (Qiagen), and cDNA was generated using a high-capacity RNA to cDNA Kit (Life Technologies).

2.6 | Cell lines and cell culture

Detailed culturing methods for human MNT-1 melanoma cells, human deeply pigmented neonatal epidermal melanocytes, and HEK293T cells are provided in Appendix S1.

2.7 | RNA isolation, reverse transcriptase-quantitative PCR

Human cell lines were harvested using Tri-Reagent solution (Ambion), and RNA was extracted using a Direct-zol RNA Miniprep Kit (Zymo Research). Complementary DNA (cDNA) was synthesized from total RNA using a high-capacity RNA to cDNA Kit (Life Technologies).

Enucleated eyes from adult mice were dissected to isolate the posterior chamber under a Leica DMC2900 stereo-microscope. The retina was carefully removed, and the cells of the choroid and RPE were scraped from the sclera and placed into RNAlater (Invitrogen). RNA was extracted using the RNAeasy Kit (Qiagen) and cDNA was synthesized utilizing SuperScript II RT (Invitrogen) with random primers. All reverse transcriptase-quantitative PCR (RT-qPCR) primers used are listed in Table S4. For additional details, see Appendix S1.

2.8 | Nanostring nCounter analysis on whole-mouse skin

RNA was isolated from mice at P60 following stimulation of 3rd Anagen as described (Paterson et al., 2015). A full description of RNA isolation and Nanostring analysis is described in Appendix S1.

For RT-qPCR analysis on skin, cDNA was synthesized as described above for cells sorted with CD117 beads.

2.9 | Identification of binding motifs and chromatin immunoprecipitation

Putative RXR/RAR binding sites in the *MITF-A* promoter were identified using MotifMap and the hg18 reference genome (Daily, Patel, Rigor, Xie, & Baldi, 2011; Xie, Rigor, & Baldi, 2009). Human NCBI accession numbers used were NM_00198159 (*MITF-A*) and NM_00248 (*MITF-M*) and corresponding mouse NCBI accession numbers are NM_002223198 (*Mitf-A*) and NM_008601 (*Mitf-M*). Conservation of the RXR/RAR binding site between human and mouse (mm10 reference genome) was determined by aligning 1,000 bp upstream of the transcription start site of *MITF-A* for the human and murine sequences in MegAlign (version 14.0.0) (DNASTAR). Two kilobases of DNA upstream of the transcription start site for each human promoter was designated as the “promoter region” and tiled using four 500 bp “tiles.” Primers for quantitative PCR targeted each of these four tiled regions are listed in Table S4 and described in Appendix S1.

2.10 | Drug treatment and dual-luciferase reporter assay

HEK293T cells were transfected with 1 µg of a firefly luciferase reporter driven by human *MITF-A* full-length promoter (*MITF-A* EcoRI) or a truncated *MITF-A* promoter (*MITF-A* SmaI). Both plasmids were a kind gift of Dr. Shigeki Shibahara as previously described (Udono et al., 2000). An additional construct with a mutagenized promoter (*MITF-A* Mut) was generated by site-specific mutagenesis (Agilent Technologies) as described in Appendix S1.

2.11 | Melanin quantification

After shaving the dorsal hairs of mice at post-natal day 50 (P50), 1 mg of hair was dissolved overnight in 1 ml of 90% Soluene-350 (PerkinElmer) and 10% water at 65°C. Quadruplicate 150 µl aliquots for each mouse hair sample were analyzed for absorbance at 405 nm as previously described (Liggins et al., 2018). Melanin quantification of tail skin was performed on 1-cm sections of whole skin dissolved in 90% Soluene-350 as described above. To measure melanin in eyes of mice, the eyes were enucleated and dissected. The iris and the posterior chamber of the eye, following removal of retina, were separated and dissolved overnight in Soluene-350 as described above.

2.12 | Histology

Eyes were collected from adult mice, and connective tissue around the eye was removed. The eyes were then fixed in 10% formalin, dehydrated in ethanol, and embedded in paraffin. Seven-micron-thick sections were dewaxed and rehydrated in ethanol and stained with hematoxylin and eosin to view general structure. Images at 20X

were taken using a Nikon Eclipse E200. High magnification images of iris were taken with a 63X oil lens on a Zeica ApoTome2.

2.13 | Western blots and immunoprecipitation

Total MITF levels were measured by generating protein lysates from both eyes of adult mice and subjecting them to immunoblotting with an MITF antibody as described in Appendix S1.

2.14 | Immunofluorescence staining

Skin and eyes were collected at P56, fixed, and embedded in optimal cutting temperature (OCT) compound, sectioned, and probed with a CD117 antibodies to identify melanocytes (see Appendix S1 for more details).

2.15 | Kidney characterization

Dissected kidneys were weighed, and one kidney per mouse was macerated to count glomeruli. Detailed methods are described in Appendix S1.

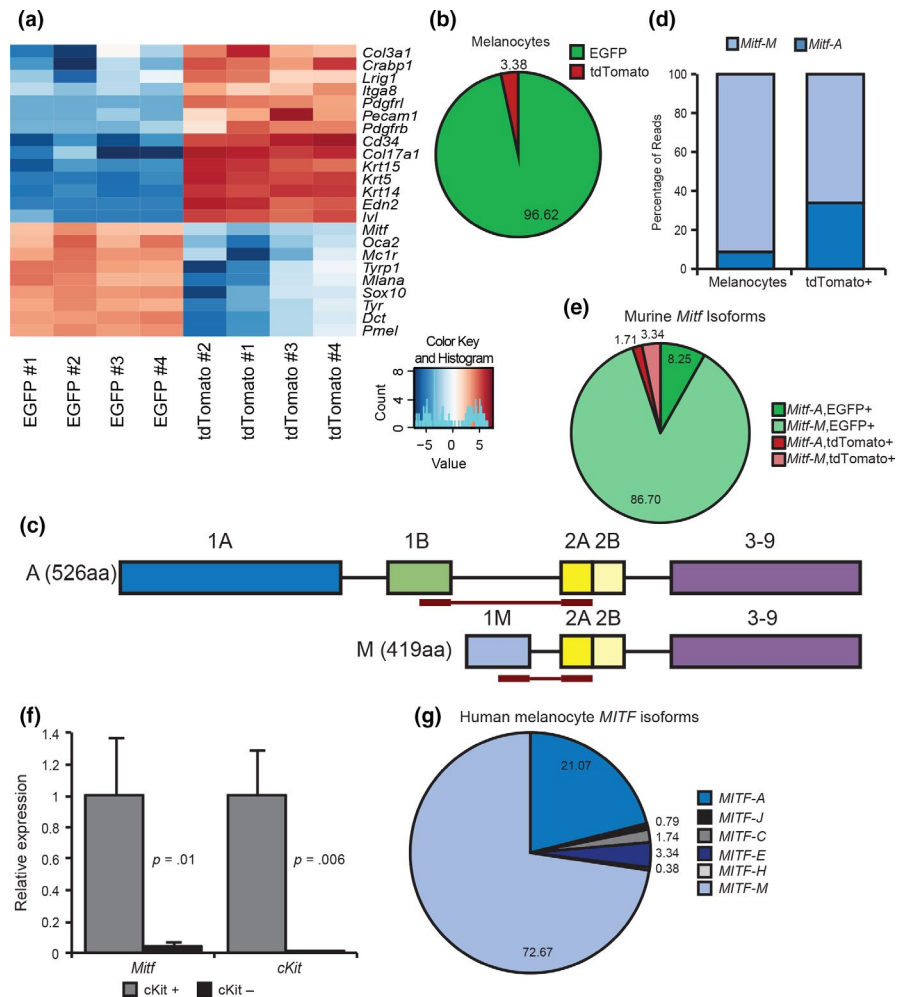
3 | RESULTS

3.1 | Multiple *Mitf* isoforms are expressed in melanocytes

To identify which *Mitf* isoforms are expressed in melanocytes, we first crossed *Tyr::Cre^{ERT2}* mice (Bosenberg et al., 2006) with *ROSA^{mtmG}* mice (Muzumdar, Tasic, Miyamichi, Li, & Luo, 2007). In *Tyr::Cre^{ERT2}*, *ROSA^{mtmG}* double heterozygous mice, injection of tamoxifen induces melanocytes to express EGFP, whereas all other cells in the epidermis express tdTomato (Figure S1a) (Liggins et al., 2018). Single-cell suspensions were generated from mouse skin of the indicated genotypes and sorted into tdTomato+ and EGFP+ populations for bulk RNA-seq. A PCA plot demonstrates that our sorting procedure could separate melanocytes from other skin cell types (Figure S1b). We next examined the expression of a panel of melanocyte, keratinocyte, fibroblast, and endothelial cell-specific transcripts in EGFP+ and tdTomato+ cells (Figure 1a, Table S1). Almost all (97%) of the transcripts encoding known melanogenesis regulators were expressed in the GFP+ sorted cells (Figure 1b). The remaining 3% of transcripts encoding melanocyte-specific markers were expressed in tdTomato+ cells, indicating that the induction of the *Tyr::Cre^{ERT2}* transgene was incomplete. In contrast, over 99% of *Trp63* transcripts (a transcription factor that regulates keratinocyte development (Mills et al., 1999; Yang et al., 1999)) were found in the tdTomato+ populations (Figure S1c), indicating that our method could efficiently sort melanocytes from other skin cells.

To determine the isoforms of *Mitf* expressed in mouse skin, BAM files for MITF transcripts were visualized and unique read junctions were counted using IGV 2.3.77 (Robinson et al., 2011; Thorvaldsdóttir et al., 2013). Read junctions between exon 1A and 1B would correspond to *Mitf-A*. Notably, no other read junctions between exon 1B

FIGURE 1 Melanocytes express multiple isoforms of *Mitf*. Cells were collected from *Tyr:Cre^{ERT2}, ROSA^{mtmG}* mice at P54 and sorted into EGFP+ and tdTomato+ populations using FACS. (a) Heatmap of RNA-seq gene expression for melanocyte-specific genes and other skin cell markers in EGFP+ and tdTomato+ cells. Transcripts range from those with high abundance (dark red) to those with low abundance (dark blue). (b) Melanocyte-specific gene expression in EGFP+ and tdTomato+ cells. (c) Schematic illustrating read junctions for *Mitf-A* and *Mitf-M*. (d) Relative distribution of *Mitf* isoforms in mouse EGFP+ melanocytes and tdTomato+ skin cell subpopulations. $n = 4$, $\chi^2 = 37,663$, $p < .0001$. (e) Distribution of *Mitf* isoforms in melanocytes and other skin cell populations of the skin. (f) Relative *Mitf* expression of cKit-positive and cKit-negative cells from neonatal epidermis sorted on microbeads. (g) *MITF* isoform relative abundance in human melanocytes



and other exons were observed in our dataset when aligned to the annotated mouse transcriptome. For simplicity, read junctions between exons 1B and 2A were counted as a proxy for *Mitf-A*, while read junctions between exons 1M and 2A were considered a proxy for *Mitf-M* (Figure 1c). In EGFP+ melanocytes, *Mitf-A* accounts for 9% of total *Mitf*, while *Mitf-M* accounts for the other 91% (Figure 1d). Of the *Mitf* expression in tdTomato+ skin cells, 66% was identified as *Mitf-M* (Figure 1d). To account for the differential expression of *Mitf* isoforms in EGFP+ and tdTomato+ cell populations, we calculated the relative abundance of these transcripts in melanocytes as compared to all other skin cells (Figure 1e). To validate RNA-seq findings, cKit+ cells (an established marker of melanocytes (Aoki et al., 2009)) were isolated from wild-type neonatal epidermis. RNA was isolated from cKit+ and cKit- cells and reverse-transcribed to quantify *Mitf* isoform expression. *Mitf* transcripts were abundant in cKit-expressing cells and largely absent in cKit-negative cells (Figure 1f), suggesting that the low levels of *Mitf* transcripts detected in tdTomato+ cells are a result of the presence of uninduced melanocytes in that sample.

To verify that both *MITF-M* and *MITF-A* are expressed in human melanocytes, we measured the relative abundance of *MITF-M* and *MITF-A* transcripts using isoform-specific RT-qPCR primers. In MNT-1-pigmented melanoma cells and deeply pigmented human melanocytes, both *MITF-M* and *MITF-A* are expressed at

similar proportions as observed in the adult mouse (Figure S1d–e). Additionally, utilizing a published human epidermal melanocyte RNA-seq dataset (Haltaufderhyde & Oancea, 2014), we determined the relative isoform abundance of *MITF* isoforms by counting read junctions as proxy for individual isoforms. Multiple isoforms containing exon 1B were identified, so read junctions between exons 1B and 2 were taken as proxy for all exon 1B containing isoforms (Figure S1f). Relative abundance for each individual isoform containing exon 1B was proportioned by counting read junctions from exons 1A, 1J, 1C, 1E, and 1H to exon 1B (Figure S1f). Read junctions between exons 1M and 2 were counted as proxy for *MITF-M* (Figure S1f). In human melanocytes, 73% of *MITF* was *MITF-M* and the next most abundant isoform was *MITF-A*, which accounted for 21% (Figure 1g). The other isoforms present accounted for less than 6% of total *MITF* expression (Figure 1g). These results confirm that *MITF-M* is the primary isoform expressed in both mouse and human melanocytes, and *MITF-A* is the second most abundant isoform expressed in melanocytes.

3.2 | The *MITF-A* promoter contains a RXR/RAR binding site

To determine how *MITF-A* is differentially regulated in melanocytes, we searched for unique binding motifs in the alternative promoters

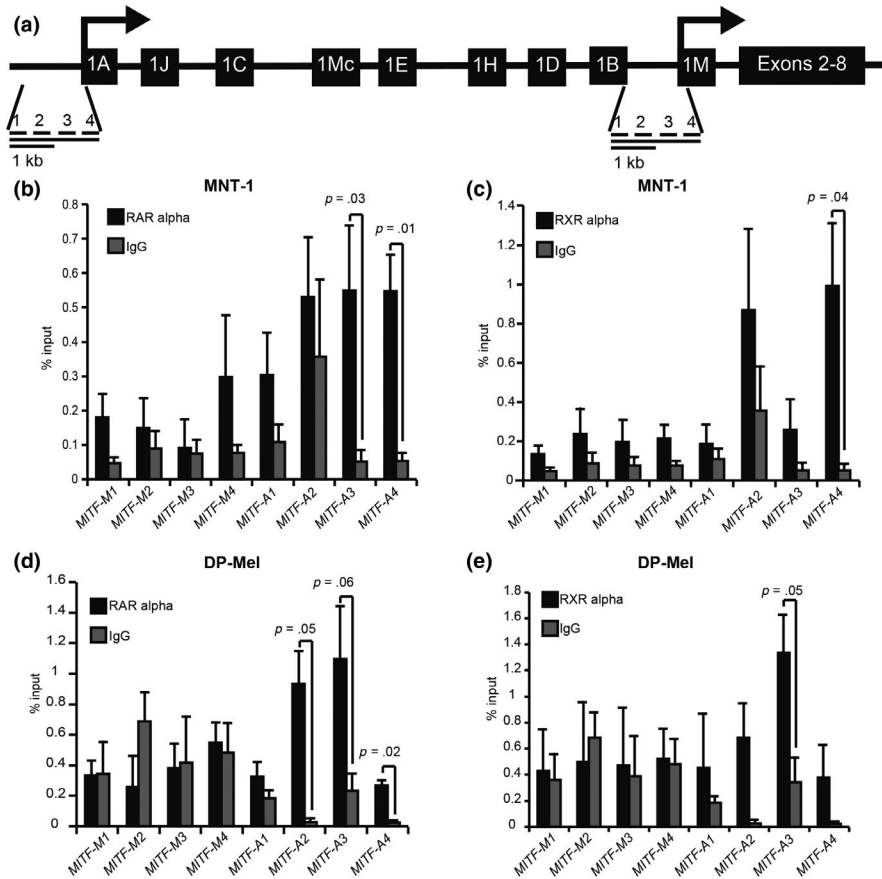


FIGURE 2 RXR/RAR binds upstream of the human *MITF-A* promoter. (a) Tiled primers for ChIP analysis were designed to target the promoter region 2 kb upstream of the transcription start site for both *MITF-A* and *MITF-M* isoforms. (b–e) Enrichment of both (b, d) RAR α and (c, e) RXR α in *MITF* promoter regions was investigated using ChIP RT-qPCR analysis in (b–c) MNT-1 cells and (d–e) darkly pigmented human melanocytes (DP-Mel), $n = 3$

for human *MITF-A* and *MITF-M*. Utilizing MotifMap (Daily et al., 2011; Xie et al., 2009), we verified the presence of known sites that mediate *MITF-M* transcription including CREB and PAX (Table S2). We also identified a putative RXR/RAR DR5 binding site 714 base pairs (bp) upstream of the transcription start for *MITF-A* (Table S3). While the promoter regions, including the RXR/RAR binding site, for the A isoform, are conserved in the mouse 740 bp upstream of the transcription start site (Figure S2), the expression of *MITF-A* is more robust in human melanocytes (Figure 1, Figure S1). We previously showed that 9-*cis* retinoic acid upregulates *MITF* and *TYR* expression in cultured melanocytes, stimulating pigment production in melanocyte and melanoma cell lines (Paterson, Ho, Kapadia, & Ganesan, 2013). Both the retinoic acid receptors (RARs) and retinoid x receptors (RXRs) form dimers that are activated in response to retinoids (Allenby et al., 1993). Additionally, RXR α is expressed in melanocytes (Reichrath et al., 1995) and a RXR α hypomorphic (I273N) mouse mutant exhibits premature graying (Du et al., 2005).

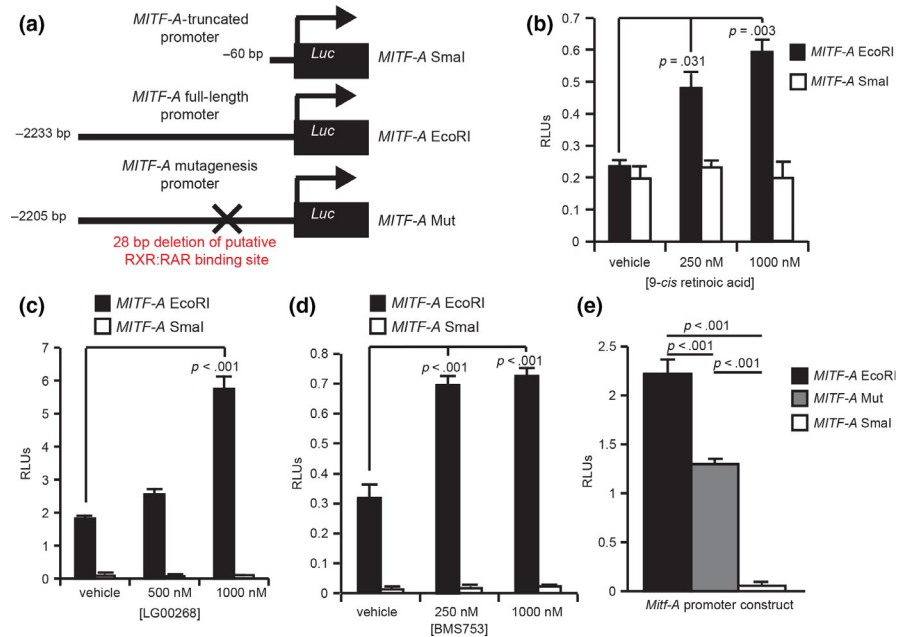
Having established that *MITF-A* expression levels were higher in human melanocytes compared with mouse, we next sought to validate the binding of RXR and RAR to the *MITF-A* human promoter. For ChIP analysis, we designed tiled primers for 2kb upstream of transcription start sites for both *MITF-A* and *MITF-M* (Figure 2a). The putative RXR/RAR DR5 binding site is located in tile A3. In the human MNT-1 melanoma cell line, we found that pulldown with RAR α significantly enriched for tiles A3 and A4 (Figure 2b) and RXR α enriched for tile A4 (Figure 2c). Using deeply pigmented (DP)

human melanocytes, tile A4 was significantly enriched with RAR α , while tiles A2 and A3 were approaching significance (Figure 2d). For RXR α in DP melanocytes, only tile A3 was approaching significance (Figure 2e). Consistent with our MotifMap findings, RAR α and RXR α did not bind to the *MITF-M* tiles (Figure 2b–e).

3.3 | Retinoids stimulate *MITF-A* promoter

Having demonstrated binding of RXR/RAR to a region within the *MITF-A* promoter, we next investigated whether RXR and RAR ligands could induce *MITF-A* promoter activity. To test the activity of the human *MITF-A* promoter, we used *MITF-A* promoter luciferase plasmid constructs containing either full-length or truncated *MITF-A* promoter (Figure 3a). Luciferase experiments were conducted in HEK293T cells. The full-length *MITF-A* promoter construct had activity similar to the truncated construct in serum-starved, vehicle (ethanol)-treated cells (Figure 3b). By contrast, 9-*cis* retinoic acid induced luciferase activity of the full-length *MITF-A* promoter construct, but failed to induce luciferase activity of the truncated *MITF-A* construct (Figure 3b). In the presence of DMSO, the vehicle for some retinoid receptor ligands, the full-length construct had a higher baseline activation compared with the truncated promoter (Figure 3c–e). Stimulation of the RXR subunit alone using the pan-RXR agonist LG100268 increased the activation of the luciferase reporter above baseline (Figure 3c), verifying that RXR can induce the luciferase activity

FIGURE 3 Retinoids stimulate the human *MITF-A* promoter through RXR/RAR binding site. (a) Schematic showing the size of *MITF-A* promoter upstream of the luciferase gene in the pGL3-luciferase plasmid constructs. (b-d) HEK293T cells were transfected with *MITF-A* promoter constructs and co-transfected with a Renilla luciferase reporter as an internal control. The cells were treated with the indicated dose of (b) 9-*cis* retinoic acid; (c) LG100268, a RXR agonist; and (d) BMS753, a RAR α -specific agonist. (e) HEK293T cells were transfected with promoter constructs including a mutant *MITF-A* promoter lacking the putative RXR/RAR binding site. $n = 3$



of this reporter. Likewise, increasing concentrations of BMS753, a potent RAR α agonist, stimulated the activity of the full-length *MITF-A* promoter construct (Figure 3d). Taken together, these results suggest that RXR/RAR heterodimers can regulate the expression of *MITF-A*. This is consistent with previous findings that 9-*cis* retinoic acid can regulate *MITF* expression (Paterson et al., 2013).

Having verified that the *MITF-A* promoter responds to retinoids, RXR, and RAR agonists, we next tested whether RXR/RAR regulates *MITF-A* expression via the newly identified RXR/RAR binding site. Using site-directed mutagenesis, we deleted 28 bp encompassing the 17 bp motif identified through MotifMap to generate a mutant promoter construct (Figure 3a). Baseline luciferase activity from the mutant construct was significantly reduced compared with the full-length promoter construct, although the mutant retained higher levels of luciferase expression when compared to the truncated promoter (Figure 3e). These results can be explained by the presence of other enhancer elements in the promoter that are known to activate *MITF-A* expression. Taken together, these studies indicate that RXR/RAR activation can induce the expression of *MITF-A*.

3.4 | *Mitf* isoform-specific mutant mice

While expression studies have defined *Mitf-M* as the melanocyte-specific isoform and *Mitf-A* as a regulator of eye development (Reinisalo, Putula, Mannermaa, Urtti, & Honkakoski, 2012), the specific function of each isoform during development is unclear. Established mouse *Mitf* mutant alleles have loss of expression or function of multiple isoforms (Steingrímsson, 2008; Steingrímsson et al., 2003, 2004), making it difficult to determine the distinct roles of *Mitf* isoforms in tissue development. Because each isoform has its own unique first exon, we sought to generate mutant mice specifically lacking a single isoform. We

designed guide RNAs for CRISPR/Cas9 gene editing for exons 1A and 1M of *Mitf*. Utilizing this technique, we generated a 7 bp deletion at the beginning of the coding region of exon 1A that produces a frameshift mutation that causes multiple premature stop codons (Figure 4a, Figure S3a,b). This allele was designated *Mitf^{em1Gane}*, but for clarity, homozygous mice will hereafter be referred to as *Mitf-A* knockout or null mice. Similarly, we also generated an 18 bp deletion spanning the splice site for exon 1M of *Mitf* (Figure 4a, S3c) designated *Mitf^{em2Gane}*. Mice homozygous for the *Mitf^{em2Gane}* allele, with targeted deletion of the *Mitf-M* isoform, will hereafter be referred to as *Mitf-M* knockout or null.

The loss of specific isoforms of *Mitf* produced distinct pigment phenotypes. While mice lacking *Mitf-A* have no visible defect on a black (non-agouti) coat-color background (Figure 4b, Figure S4a–b, S5a–b), quantitative analysis of the hair detected a 7% reduction in melanin accumulation of *Mitf-A* knockout mice compared with wild-type black mice (Figure 4c). In contrast, mutation of *Mitf-M* results in a loss of melanin in the hair and the skin of the ears and tail similar to the phenotype seen in albino mice (Figure 4d–f, Figure S4c–d, S5c–d). Despite this dramatic loss of coat color, *Mitf-M* knockout mice are distinct from albino mice since their eyes contain some pigment and appear dark (Figure 4d, Figure S5c). Other studies have shown that mice heterozygous for mutations in the *Mitf* promoter region do not have appreciable differences in coat color (Steingrímsson et al., 2003). Similarly, the loss of one copy of *Mitf-M* does not result in an appreciable change in pigmentation as mice appear black (Figure 4d). Moreover, there were no quantifiable differences in pigmentation in these animals, as they accumulate similar amounts of melanin in their hair as wild-type mice (Figure 4e).

Previous studies have shown that overexpression of *Mitf-A* in kidneys can increase the ratio of kidney to body mass and increase the number of glomeruli, while the deletion of *Mitf-A* and elements upstream of the *Mitf-A* promoter results in experimental mice with kidneys that have less glomeruli (Phelep et al., 2017). Histological

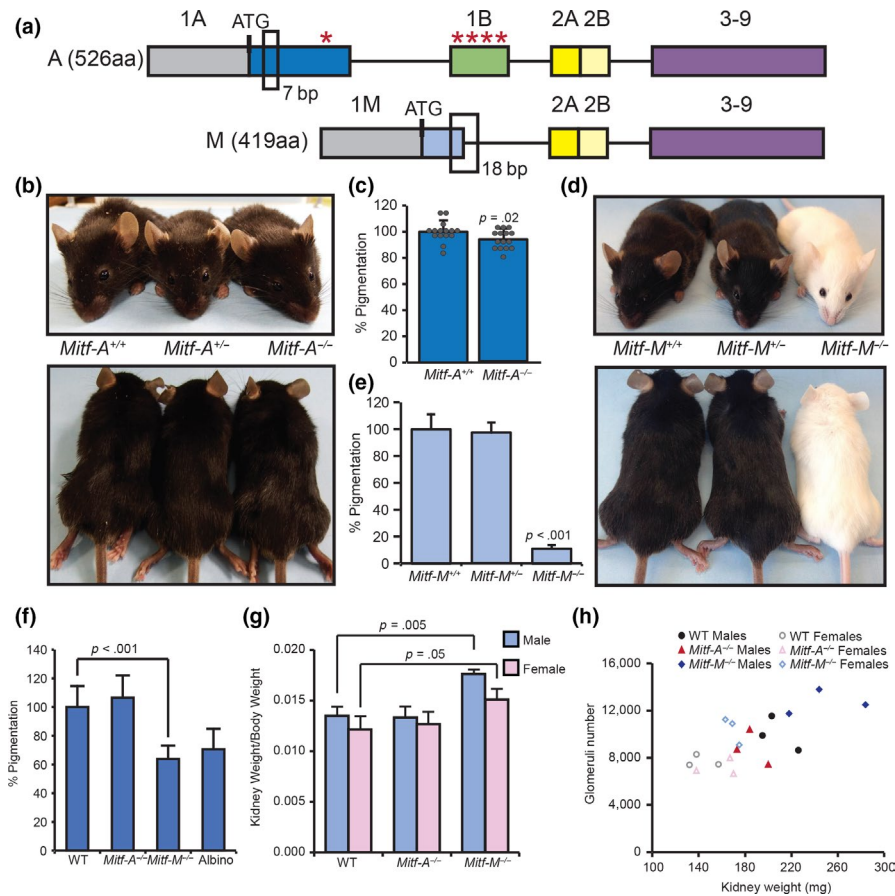


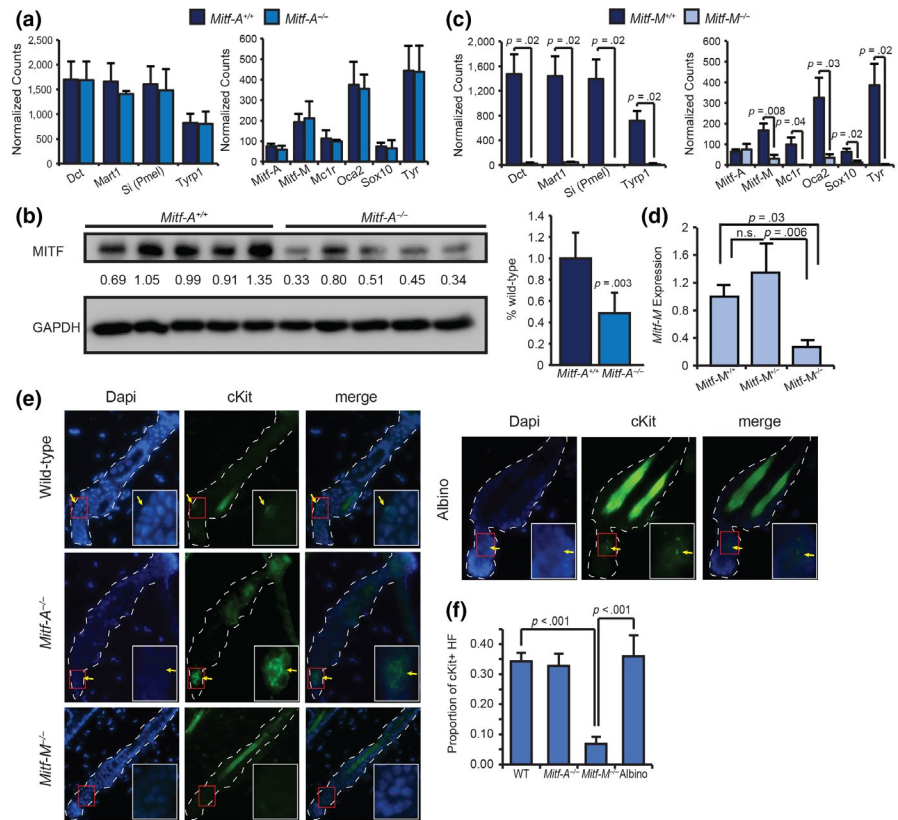
FIGURE 4 *Mitf-A* and *Mitf-M* isoform-specific mutant mice generated using CRISPR/Cas9 gene targeting platform. (a) Schematic of 7 bp deletion in exon 1A for *Mitf-A* knockout mice and 18 bp deletion in exon 1M and intron for *Mitf-M* knockout mice. Untranslated regions of exons 1A and 1M are gray, while coding regions are blue. Red asterisks denote premature stop codons in first 2 exons caused by 7 bp deletion. (b) Wild-type and *Mitf-A* isoform-specific knockout heterozygous and homozygous mice imaged at p50. (c) Melanin quantification of hair collected at p50 normalized to wild-type mice. $n = 15$. (d) Comparison of wild-type and *Mitf-M* isoform-specific knockout heterozygous and homozygous mice imaged at p50. (e) Melanin quantification of hair collected at p50 normalized to wild-type mice. $n = 10$. (f) Melanin quantification on tail skin of wild-type, *Mitf-A*^{-/-}, *Mitf-M*^{-/-}, and B6 albino mice. (g) Quantification of total kidney mass to body mass for males and females of indicated genotypes, $n = 3$. (h) Scatterplot of glomeruli number and kidney weight for individual male (filled shapes) and female (open shapes) of wild-type (circles), *Mitf-A*^{-/-} (triangles), and *Mitf-M*^{-/-} (diamonds) mice

analysis of kidneys from our *Mitf-A* null, 4-month-old mice showed no gross morphological changes as determined by two separate pathologists (Figure S6a–d). Additionally, in our mice, the loss of *Mitf-A* did not significantly alter the ratio of kidney to body mass (Figure 4f, Figure S6e) or the number of glomeruli in the kidney (Figure 4g, Figure S5e). The melanocyte-specific isoform *Mitf-M* was also detected in the kidneys (Figure S6f–g) and loss did significantly increase the ratio of kidney to body mass in both males and females (Figure 4f). However, while there was a trend toward increased glomeruli in *Mitf-M* knockout mice, the difference was not significant (Figure 4g, Figure S6e). In *Mitf-M* knockout mice, there was no significant change in relative isoform abundance with the exception of *Mitf-A* and total *Mitf* (Figure S6f); however, there is a trend toward enrichment of the *Mitf-C* isoform with the loss of *Mitf-M* in the kidney (Figure S6g).

To more closely examine the expression of melanocyte isoforms of *Mitf* in the skin, we examined melanocyte-specific gene

expression in whole back skin from wild-type and isoform-specific knockout mice using Nanostring. *Mitf-A* knockout mice had a similar gene expression profile compared with wild-type mice (Figure 5a). While the 7 bp deletion causes a frameshift (Figure S3b), it did not alter the stability of the mRNA transcript, and *Mitf-A* expression levels were unchanged in knockout mice. To verify that the *Mitf-A* knockout mice lack functional MITF-A protein, we collected protein lysate from whole eyes of wild-type and *Mitf-A* knockout mice, as *Mitf-A* is the predominant isoform in the eye. *Mitf-A* knockout mice had ~50% reduced levels of total MITF in the eye (p -value = .003; Figure 5b). Consistent with the visual loss of pigmentation, *Mitf-M* knockout mice had decreased the expression of all melanocyte-specific genes in the skin without notable changes in the expression of *Mitf-A* (Figure 5c). Mice heterozygous for the *Mitf-M* mutation showed no significant change in *Mitf-M* expression using RT-qPCR (Figure 5d), suggesting that the wild-type allele is upregulated in *Mitf-M* heterozygotes. RT-qPCR was not sensitive enough to detect

FIGURE 5 *Mitf* isoform-specific knockout mice have distinct skin gene expression phenotypes. Skin was collected at P60 for RNA extraction after stimulating the hair cycle at P50. Purified RNA was subjected to Nanostring analysis on melanocyte-specific genes. Data shown are mean normalized counts of mRNA for each gene in (a) *Mitf-A* knockout mice and (c) *Mitf-M* knockout mice compared with wild-type littermates. Wild-type, *Mitf-M*^{-/-} *n* = 3; *Mitf-A*^{-/-} *n* = 2. (b) Western blot for pan-Mitf on whole-eye protein lysates from *Mitf-A*^{+/+} and *Mitf-A*^{-/-} mice. (d) Relative expression of *Mitf-M* in *Mitf-M* wild-type, heterozygous, and knockout mice. (e) cKit staining on indicated mouse skin collected at P56 with cKit-positive melanocytes indicated by arrows and bounded by the red box, inset. (f) Quantification of cKit-positive hair follicles (HF), *n* = 3



the different isoforms of *Mitf* expressed in the skin. This type of the analysis would likely require isolation of melanocytes from the skin to generate enough *Mitf* transcripts that could be reproducibly measured. We did note that the downregulation of melanogenesis markers in *Mitf-M* knockout mice coincides with the loss of cKit-positive melanocytes in the hair follicle (Figure 5e–f). This loss of cKit-positive cells was observed in *Mitf-M* knockout mice, but not in *Mitf-A* null or albino mice, suggesting that the pigment phenotype observed in these mice is secondary to the loss of melanocytes.

During normal development, MITF controls the migration of melanoblasts to target tissues including the epidermal basal membrane, the hair follicle, the iris stroma, and the choroid of the eye (Vachtenheim & Ondrusov, 2013). Choroidal and iris stromal melanocytes and the pigmented epithelia of the iris (IPE) and retina (RPE) are thought to rely on MITF to induce melanin production. Unlike the neural crest-derived melanocytes, the cells of the pigmented epithelium are derived from the optic cup and express multiple isoforms of *Mitf* (Bharti, Nguyen, Skuntz, Bertuzzi, & Arnheiter, 2006). Because these distinct pigment layers in the eye rely on different isoforms of *Mitf*, we investigated whether *Mitf* isoform-specific knockout mice had any eye phenotype. Live animal images taken of mice suggest a subtle loss of pigment in the iris of *Mitf-M* knockout mice (Figure 6a (top), Figure S7a–d). There was a significant reduction (~35%) in pigmentation in the iris of *Mitf-M* knockout mice (Figure 6b) when melanin absorbance of the isolated iris was quantified. In contrast, *Mitf-A* knockout mice had no significant change in iris pigmentation (Figure 6b). Moreover, the difference in iris pigmentation was somewhat apparent when hematoxylin and eosin (H&E)-stained sections

were visualized at 20× magnification (Figure S8a–d), and even more apparent when these sections were visualized at 63× magnification (Figure S8e–h). Upon enucleation of the eyes, it became apparent that the loss of *Mitf-M*, but not *Mitf-A*, affected pigment accumulation in the posterior of the eye (Figure 6a, Figure S7e–h), a result that was even more evident after removal of the retina from the posterior segment. Overall, the posterior segment of the eye of *Mitf-M* knockout mice had 30% of the pigment present in wild-type eyes as measured by relative melanin absorbance (Figure 6c). *Mitf-M* knockout mice did have significantly more pigment in their eyes when compared to B6 albino mice (Figure 6b–c), which are known to lack pigment in both melanocytes and the retinal pigment epithelium. H&E staining of wild-type and *Mitf-A* knockout mice revealed pigmentation in both the choroid and RPE; however, the loss of *MITF-M* results in the loss of choroidal pigmentation while the RPE appears normally pigmented (Figure 6d, Figure S8i–l). Choroidal cKit-positive melanocytes are also absent in *Mitf-M* knockout mice (Figure 6e). While histology reveals no gross morphological defects in the retina, we next sought to ensure any phenotypes observed in the *Mitf* knockout mice are not due to changes in retinal degeneration caused by the presence of the *Crb1 rd8* mutation from the C57BL/6N line. Since the *Mitf-A* and *Mitf-M* lines are on a mixed 6N and 6J background, 50 mice of each line were genotyped for the *Crb1* wild-type and *rd8* alleles. Primers were validated with C57BL/6J mice, which lack the *rd8* mutation, and C57BL/6N, which are homozygous for the *rd8* mutation. The *Mitf-M* mice tested in these studies were all either heterozygous or lack the *rd8* allele altogether. Their eye phenotypes were compared against the eyes of wild-type mice, including those

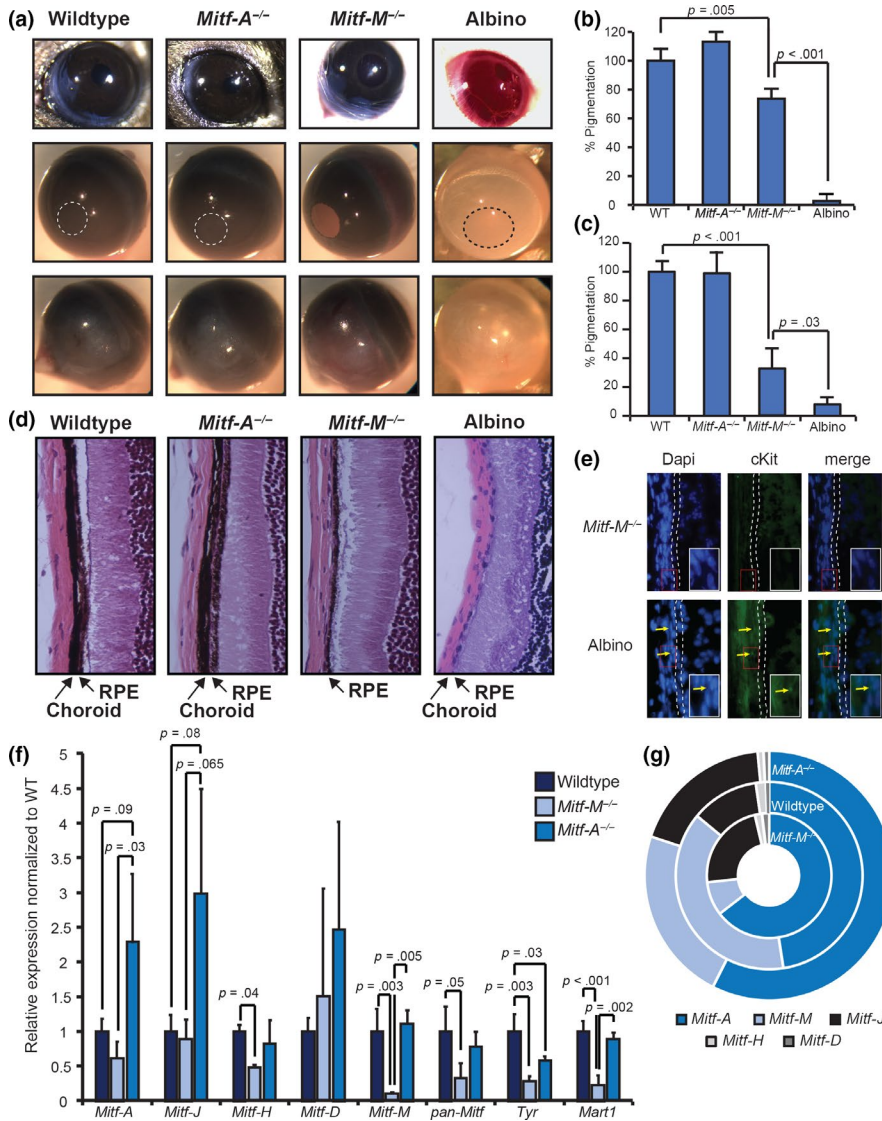


FIGURE 6 *Mitf* isoform-specific knockout mice have distinct eye phenotypes. (a) Representative images of whole eyes of indicated mice before (top) and following enucleation of iris with pupil indicated (middle) and posterior surface of the eye (bottom). (b) Melanin quantification on dissected iris of indicated mice, $n = 3$. (c) Pigment assay on combined RPE, choroid, and sclera of wild-type, *Mitf-A*^{-/-}, *Mitf-M*^{-/-}, and Albino mice, $n = 4$. (d) H&E sections from paraffin-embedded eyes with choroid and RPE indicated by arrows. (e) cKit staining of choroid, with RPE highlighted and cKit-positive melanocytes indicated with arrows. The inset area is highlighted by the red box. (f) Relative expression of *Mitf* isoforms in the isolated RPE and choroid of wild-type and *Mitf* isoform-specific mutant mice, $n = 3$. (g) Further comparison of *Mitf* isoform abundance in the RPE and choroid of wild-type and *Mitf* knockout mice

from the C57BL/6N line, which are known to be homozygous for *rd8*. Given these results, it is highly unlikely that the phenotypes observed are related to *rd8*, as none of the *Mitf-M* mice examined were *rd8* homozygotes while, in contrast, the control mice examined were *rd8* homozygotes (Figure S7i-j). Using RT-qPCR, we compared the expression of isoforms in the combined choroid and RPE of the mice. The mutation in *Mitf-M* resulted in the expected downregulation of the *Mitf-M* transcript as well as total *Mitf*, *Tyr*, and *Mart1* (Figure 6f). In *Mitf-A* knockout mice, there was an increase in the mutated *Mitf-A* transcript that results in premature stop codons. The mutation was verified using Sanger sequencing of wild-type and knockout *Mitf-A* transcripts (Figure S9). Interestingly, more *Mitf-J* transcripts also accumulated in *Mitf-A* knockout eyes when compared to the choroid and RPE of wild-type mice. These changes in specific transcripts are highlighted by the change in relative abundance of *Mitf* isoforms in the eye (Figure 6g). Finally, we also observed decreased accumulation of *Tyr* transcript in *Mitf-A* knockout eyes (Figure 6f), consistent with other studies that indicate that MITF-A regulates *TYR* expression in the eye (Amae et al., 1998). Together, these studies show that

the deletion of *Mitf-A* or *Mitf-M* has distinct effects on the development of the skin, eyes, and kidneys.

4 | DISCUSSION

The use of alternative promoters by a gene enables more sophisticated control of the gene's expression. Such elaboration helps facilitate development and tissue specification, and is also associated with unique disease states (Davuluri et al., 2008). In the eye, mouse *Mitf* isoforms are known to be differentially regulated during the formation of the RPE (Bharti et al., 2008). We show here that the expression of *MITF-A*, the second most abundant isoform in human melanocytes (Figure 1), is regulated by retinoids, transcriptional activators that have a prominent role in eye development (McBee, Palczewski, Baehr, & Pepperberg, 2001). Retinoids can regulate alternative promoters. The *Strat6* gene contains two alternative promoters, with the intronic promoter containing a retinoic acid response element (RARE). Under excessive vitamin A levels, there is

increased expression of *Strab5* from the intronic promoter (Laursen, Kashyap, Scandura, & Gudas, 2015). Similarly, it is conceivable that levels of retinoids may dictate *MITF* isoform expression within the RPE, as retinoids are known regulators of eye development.

Our group has shown that 9-*cis* retinoic acid and retinal stimulate melanogenesis in pigmented cell lines (Paterson et al., 2013), while others have shown that retinal increases the sensitivity of melanocytes to UVA-induced pigment production (Wicks, Chan, Najera, Ciriello, & Oancea, 2011). Based on the finding that 9-*cis* retinoic acid led to an upregulation in *MITF* expression (Paterson et al., 2013), we identified a RARE binding motif in the human *MITF* promoter upstream of the 1A exon. Apart from the *MITF-M* promoter, the regulators of other isoform-specific promoters are poorly understood (Steingrímsson, 2008). While it is possible that the RARE facilitates chromatin looping to regulate distant genes or additional *MITF* isoforms, we have shown this binding motif contributes to human *MITF-A* promoter activity (Figure 3). Consistent with this notion, retinoid receptors have also been linked to pigmentation. A germline mutation of RXR α in the RXR α ^{pke} mouse results in premature graying starting when mice reach 5 weeks (Du et al., 2005). RXR α ^{pke} mice also experience alopecia and are hairless at 4 months (Du et al., 2005), so the isolated effect of RXR α on melanocytes and pigmentation is still unknown. Conditional deletion of RXR α in keratinocytes causes a dilute coat color (Li et al., 2001), suggesting that RXR α may regulate pigmentation in a melanocyte cell-autonomous and non-autonomous manner. Taken together, these results indicate that the deletion of *MITF-A* in melanocytes, like the RXR α knockout, only partially affects hair follicle pigmentation.

In humans, mutations in *MITF* have been linked to Waardenburg syndrome, type 2A and Tietz syndrome, and disorders characterized by pigmentary defects including a white forelock and hearing loss (Pingault et al., 2010; Wildhardt et al., 2013). These mutations occur throughout the *MITF* gene, but are most common in the DNA-binding domains (Grill et al., 2013) with some of the mutations recapitulated in mice (Pingault et al., 2010). Similarly, mutations in humans associated with familial melanoma and predisposition to renal cell carcinoma (Bertolotto et al., 2011; Grill et al., 2013) are also within the DNA-binding domains. The characterized mouse mutations in *Mitf* only partially recapitulate pigmentary disorders, but cause a wide range of phenotypes including pigmentation defects, microphthalmia, hearing loss, changes in bone density, and deficiency in immune cells (Steingrímsson et al., 2004). The majority of mouse mutations occur in the DNA-binding and dimerization domains that can alter all isoforms of *MITF*, which explains the wide range of tissues affected (Steingrímsson et al., 2004). Even mutations in the promoter regions have variable phenotypes. Both the *Mitf*^{mi-vga9}, a *MITF* null, and *Mitf*^{mi-rw} mice, which has a deletion of multiple unique first exons and promoter regions, have pigmentation and eye defects found only in homozygous mice (Hodgkinson et al., 1993; Watanabe et al., 2002). To distinguish the role of different isoforms, we generated *Mitf-A* and *Mitf-M* isoform-specific knockout mice. These unique specific isoform knockout reagents can be used to better delineate the function of individual isoforms, as described in this manuscript.

While *Mitf-A* was first thought to play an important role in the development of the RPE (Amae et al., 1998), similar to the loss of *Mitf-D* and *Mitf-H* in the *Mitf*^{mi-rw} mouse (Bharti et al., 2008), we found that *Mitf-A* is not required for the development of the RPE (Figure 6). These results suggest that though *Mitf-A* plays a role in pigmentation of the hair and eye (Figures 4–6), it is redundant in melanocytes and both the IPE and RPE cells. Lack of a phenotype in the RPE may be a result of compensation by additional *Mitf* isoforms, as was shown with the loss of *Mitf-D* (Bharti et al., 2012). Since *Mitf-A* is expressed in multiple tissues (Amae et al., 1998), the A isoform may have more specific roles in other organs such as the kidney, where the overexpression of *Mitf-A* caused an increase in size and nephron number while the deletion of the promoter and *Mitf-A* decreases the glomeruli number (Phelep et al., 2017). In our study, we found no significant change in kidney mass in our *Mitf-A* knockout mice (Figure 4, Figure S5). This difference in phenotype may be secondary to the deletion of almost 6,000 bp that includes exon 1A and the *Mitf-A* promoter in Ref. (Phelep et al., 2017) as compared to the more specific deletion within the 1A exon presented in this study. Since the *Mitf* isoforms can be regulated by distant regulatory elements, large changes in the promoter regions may modulate the expression of multiple isoforms, as observed in mice with the *Mitf*^{vga9} allele. In contrast, exon-specific deletions could affect promoter regulation in cases where *Mitf* isoforms themselves differentially activate *Mitf* promoters. Future studies will address the broad impacts of loss of individual *Mitf* isoforms on the expression of other *Mitf* isoforms and *Mitf* target genes at different times during development.

The loss of *Mitf-M* results in the loss of melanocytes in the hair, skin, iris stroma, and choroid, but not the cells of the IPE and RPE (Figures 4–6). This phenotype is similar to the phenotype of *Mitf*^{mi-bw} mice, where a LINE1 element is inserted between the common exons 3 and 4 (Hozumi et al., 2012; Yajima et al., 1999). While the *Mitf*^{mi-bw} mice have the loss of *Mitf-M* expression in the skin and eye, the LINE insertion also results in reduced expression and alternatively spliced transcripts of *Mitf-A* and *Mitf-H* (Yajima et al., 1999). During embryonic development, aberrant *Mitf-M* transcripts were also detected (Takeda et al., 2014), indicating the *Mitf*^{mi-bw} allele is not a clean knockout of the M isoform. *Mitf-M* heterozygotes have no pigment defects (Figure 4d–e), which suggests that one copy of *Mitf-M* is sufficient to maintain *Mitf-M* expression levels (Figure 5d). In this study, we have generated a specific *Mitf-M* knockout mouse and demonstrated that the loss of *MITF-M* results in the loss of iris stromal and choroidal melanocytes. Our findings also demonstrate that while *Mitf-M* may be expressed in the adult RPE (Maruotti, Thein, Zack, & Esumi, 2012) and can rescue the loss of pigmentation in *Mitf*^{vga9} mice (Michael et al., 2018), it is not required for pigmentation of the RPE. Additionally, the loss of *Mitf-M* increased the size of the kidneys (Figure 4), indicating that the loss of a single isoform affects distinct tissues differently, further highlighting the utility of the isoform-specific knockout reagents generated in this study.

Recent studies in the eye have identified the *Crb1* mutant *rd8* allele present in the C57BL/6N mice as a cause of retinal degeneration (Mattapallil et al., 2012; Moore et al., 2018). While the *rd8* allele is

present in both of the knockout lines from the original C57BL/6NTac embryos, both lines were outcrossed to C57BL/6J to isolate individual CRISPR alleles. In the 50 mice from the *Mitf-M* line studied here, all were either wild-type or heterozygous for the *rd8* allele at the *Crb1* locus (Figure S7j). Published studies have shown that *rd8* heterozygous mice show no signs of retinal degeneration as compared to *rd8* homozygous mice (Luhmann et al., 2015). In this study, eye phenotype comparisons were made between *Mitf-M* knockout mice and C57BL/6N mice, which are homozygous for the *rd8* allele. While we cannot exclude that the *rd8* allele can influence the RPE phenotypes observed here, it is unlikely that our observed results are caused by an *rd8* mutation. Moreover, *Mitf-M* knockout mice not only have a pigment phenotype in the choroid but also in the iris stroma, further evidence that the phenotype observed here is independent of *rd8* mutation.

In summary, this study demonstrates that differential regulation of *MITF* isoforms plays a critical role in tissue development. *MITF-A* is regulated by retinoids, signaling molecules that are crucial in eye development, yet *Mitf-A* knockout mice have no eye phenotype although they have reduced *MITF* protein levels. These findings suggest that low levels of *MITF* are likely required for RPE pigmentation and *Mitf* isoforms play redundant roles in this process. In contrast, *Mitf-M* deletion results in the loss of melanocytes in both the skin and choroid, indicating that this isoform is necessary for melanocyte development in these tissues. This work provides a first glimpse at how two distinct *Mitf* isoforms regulate three distinct tissues and is another example of how protein isoforms can be differentially regulated in tissues, resulting in distinct developmental phenotypes that influence human disease.

ACKNOWLEDGEMENTS

We thank Kai-Xuan Shi and Shuling Wang of the UCI Transgenic Mouse Facility (TMF) for pronuclear injection and molecular analysis, respectively, for the production of *Mitf-A* and *Mitf-M* CRISPR knockout mice. We thank Dr. Shigeki Shibahara for his kind gift of the *MITF-A* luciferase plasmid constructs and Feng Zhang for his kind gift of the pX330-U6-Chimeric_BB-CBh-hSpCas9 plasmid. We thank Sahil Telang and Madeline McCanne for assistance with luciferase assays and Yumay Chen for examining kidney histology. We thank Amber Habowski, Chi-Fen Chen, Jessica Shiu, and Klemens Hertel for advice on experimental design and editing the manuscript. We thank the UCI Genomics High Throughput Facility (GHTF) for their help with Nanostring nCounter and RNA sequencing. We thank the Institute for Immunology Flow Cytometry Core Facility (FCCF) for assistance with sorting cells using FACS. This work was supported by grants from the National Institutes of Health (R01AR063116, R01CA151513, and U54-CA217378) to AKG. The research reported in this publication was supported by the National Cancer Institute of the National Institutes of Health Award Number T32CA009054-37 and an Anti-Cancer Challenge research grant from the University of California, Irvine Chao Family Comprehensive Cancer Center to JLF. The TMF, GHTF, and FCCF are Shared Resources funded in part by the Chao Family Comprehensive Cancer Center Support Grant (P30CA062203) from the National Cancer Institute and NIH Shared

Instrumentation Grants (1S10RR025496-01, 1S10OD010794-01, and 1S10OD021718-01). The content is solely the responsibility of the authors and does not necessarily represent the official views of the National Institutes of Health.

CONFLICT OF INTEREST

The authors have no conflicts of interest to declare.

ORCID

Anand K. Ganesan  <https://orcid.org/0000-0003-4944-9274>

REFERENCES

- Allenby, G., Bocquel, M. T., Saunders, M., Kazmer, S., Speck, J., Rosenberger, M., ... Chambon, P. (1993). Retinoic acid receptors and retinoid X receptors: Interactions with endogenous retinoic acids. *Proceedings of the National Academy of Sciences*, *90*(1), 30–34. <https://doi.org/10.1073/pnas.90.1.30>
- Amae, S., Fuse, N., Yasumoto, K.-I., Sato, S., Yajima, I., Yamamoto, H., ... Shibahara, S. (1998). Identification of a novel isoform of microphthalmia-associated transcription factor that is enriched in retinal pigment epithelium. *Biochemical and Biophysical Research Communications*, *247*(3), 710–715. <https://doi.org/10.1006/bbrc.1998.8838>
- Aoki, H., Yamada, Y., Hara, A., Kunisada, T., Kunisada, T., Pavan, W. J., & Arnheiter, H. (2009). Two distinct types of mouse melanocyte: differential signaling requirement for the maintenance of non-cutaneous and dermal versus epidermal melanocytes. *Development (Cambridge, England)*, *136*(15), 2511–2521. <https://doi.org/10.1242/dev.037168>
- Arsic, N., Gadea, G., Lagerqvist, E. L., Busson, M., Cahuzac, N., Brock, C., ... Roux, P. (2015). The p53 isoform $\Delta 133p53\beta$ promotes cancer stem cell potential. *Stem Cell Reports*, *4*(4), 531–540. <https://doi.org/10.1016/j.stemcr.2015.02.001>
- Bertolotto, C., Lesueur, F., Giuliano, S., Strub, T., de Lichy, M., Bille, K., ... Bressac-de Paillerets, B. (2011). A SUMOylation-defective *MITF* germline mutation predisposes to melanoma and renal carcinoma. *Nature*, *480*(7375), 94–98. <https://doi.org/10.1038/nature10539>
- Bharti, K., Gasper, M., Ou, J., Brucato, M., Clore-Gronenborn, K., Pickel, J., & Arnheiter, H. (2012). A regulatory loop involving PAX6, *MITF*, and WNT signaling controls retinal pigment epithelium development. *PLoS Genetics*, *8*(7), e1002757. <https://doi.org/10.1371/journal.pgen.1002757>
- Bharti, K., Liu, W., Csermely, T., Bertuzzi, S., & Arnheiter, H. (2008). Alternative promoter use in eye development: The complex role and regulation of the transcription factor *MITF*. *Development (Cambridge, England)*, *135*(6), 1169–1178. <https://doi.org/10.1242/dev.014142>
- Bharti, K., Nguyen, M. T. T., Skuntz, S., Bertuzzi, S., & Arnheiter, H. (2006). The other pigment cell: Specification and development of the pigmented epithelium of the vertebrate eye. *Pigment Cell Research*, *19*(5), 380–394. <https://doi.org/10.1111/j.1600-0749.2006.00318.x>
- Bosenberg, M., Muthusamy, V., Curley, D. P., Wang, Z., Hobbs, C., Nelson, B., ... Chin, L. (2006). Characterization of melanocyte-specific inducible Cre recombinase transgenic mice. *Genesis*, *44*(5), 262–267. <https://doi.org/10.1002/dvg.20205>
- Cong, L., Ran, F. A., Cox, D., Lin, S., & Barretto, R. (2013). Multiplex genome engineering using CRISPR/Cas systems. *Multiplex Genome Engineering Using CRISPR/Cas Systems*, *339*(6121), 819–823. <https://doi.org/10.1126/science.1231143>
- Daily, K., Patel, V. R., Rigor, P., Xie, X., & Baldi, P. (2011). MotifMap: Integrative genome-wide maps of regulatory motif sites for

- model species. *BMC Bioinformatics*, 12(1), 495. <https://doi.org/10.1186/1471-2105-12-495>
- Davis, W., & Schultz, R. M. (2000). Developmental change in TATA-box utilization during preimplantation mouse development. *Developmental Biology*, 218(2), 275–283. <https://doi.org/10.1006/DBIO.1999.9486>
- Davuluri, R. V., Suzuki, Y., Sugano, S., Plass, C., & Huang, T.-H.-M. (2008). The functional consequences of alternative promoter use in mammalian genomes. *Trends in Genetics*, 24(4), 167–177. <https://doi.org/10.1016/j.tig.2008.01.008>
- Du, X., Tabeta, K., Mann, N., Crozat, K., Mudd, S., & Beutler, B. (2005). An essential role for Rxr alpha in the development of Th2 responses. *European Journal of Immunology*, 35(12), 3414–3423. <https://doi.org/10.1002/eji.200535366>
- Edgar, R., Domrachev, M., & Lash, A. E. (2002). Gene Expression Omnibus: NCBI gene expression and hybridization array data repository. *Nucleic Acids Research*, 30(1), 207–210. <https://doi.org/10.1093/nar/30.1.207>
- Godwin, L. S., Castle, J. T., Kohli, J. S., Goff, P. S., Cairney, C. J., Keith, W. N., ... Bennett, D. C. (2014). Isolation, culture, and transfection of melanocytes. In *Current protocols in cell biology* (pp. 1.8.1–1.8.20). Hoboken, NJ, USA: John Wiley & Sons, Inc. <https://doi.org/10.1002/0471143030.cb0108s63>
- Grill, C., Bergsteinsdóttir, K., Ögmundsdóttir, M. H., Pogenberg, V., Schepsky, A., Wilmanns, M., ... Steingrímsson, E. (2013). MITF mutations associated with pigment deficiency syndromes and melanoma have different effects on protein function. *Human Molecular Genetics*, 22(21), 4357–4367. <https://doi.org/10.1093/hmg/ddt285>
- Haltaufderhyde, K. D., & Oancea, E. (2014). Genome-wide transcriptome analysis of human epidermal melanocytes. *Genomics*, 104(6), 482–489. <https://doi.org/10.1016/j.ygeno.2014.09.010>
- Hodgkinson, C. A., Moore, K. J., Nakayama, A., Steingrímsson, E., Copeland, N. G., Jenkins, N. A., & Arnheiter, H. (1993). Mutations at the mouse microphthalmia locus are associated with defects in a gene encoding a novel basic-helix-loop-helix-zipper protein. *Cell*, 74(2), 395–404. [https://doi.org/10.1016/0092-8674\(93\)90429-T](https://doi.org/10.1016/0092-8674(93)90429-T)
- Hozumi, H., Takeda, K., Yoshida-Amano, Y., Takemoto, Y., Kusumi, R., Fukuzaki-Dohi, U., ... Shibahara, S. (2012). Impaired development of melanoblasts in the black-eyed white Mitfmi-bw mouse, a model for auditory-pigmentary disorders. *Genes to Cells*, 17(6), 494–508. <https://doi.org/10.1111/j.1365-2443.2012.01603.x>
- Kim, S., & An, S. S. A. (2016). Role of p53 isoforms and aggregations in cancer. *Medicine*, 95(26), e3993. <https://doi.org/10.1097/MD.0000000000003993>
- Landry, J.-R., Mager, D. L., & Wilhelm, B. T. (2003). Complex controls: The role of alternative promoters in mammalian genomes. *Trends in Genetics*, 19(11), 640–648. <https://doi.org/10.1016/j.tig.2003.09.014>
- Laursen, K. B., Kashyap, V., Scandura, J., & Gudas, L. J. (2015). An alternative retinoic acid-responsive Stra6 promoter regulated in response to retinol deficiency. *The Journal of Biological Chemistry*, 290(7), 4356–4366. <https://doi.org/10.1074/jbc.M114.613968>
- Levy, C., Khaled, M., & Fisher, D. E. (2006). MITF: Master regulator of melanocyte development and melanoma oncogene. *Trends in Molecular Medicine*, 12(9), 406–414. <https://doi.org/10.1016/j.molmed.2006.07.008>
- Li, M., Chiba, H., Warot, X., Messaddeq, N., Gérard, C., Chambon, P., & Metzger, D. (2001). RXR-alpha ablation in skin keratinocytes results in alopecia and epidermal alterations. *Development (Cambridge, England)*, 128(5), 675–688.
- Liggins, M. C., Flesher, J. L., Jahid, S., Vasudeva, P., Eby, V., Takasuga, S., ... Ganesan, A. K. (2018). PIKfyve regulates melanosome biogenesis. *PLoS Genetics*, 14(3). <https://doi.org/10.1371/journal.pgen.1007290>
- Luhmann, U. F. O., Carvalho, L. S., Holthaus, S.-M.-K., Cowing, J. A., Greenaway, S., Chu, C. J., ... Ali, R. R. (2015). The severity of retinal pathology in homozygous Crb1rd8/rd8 mice is dependent on additional genetic factors. *Human Molecular Genetics*, 24(1), 128–141. <https://doi.org/10.1093/hmg/ddu424>
- Maruotti, J., Thein, T., Zack, D. J., & Esumi, N. (2012). MITF-M, a 'melanocyte-specific' isoform, is expressed in the adult retinal pigment epithelium. *Pigment Cell & Melanoma Research*, 25(5), 641–644. <https://doi.org/10.1111/j.1755-148X.2012.01033.x>
- Mattapallil, M. J., Wawrousek, E. F., Chan, C.-C., Zhao, H., Roychoudhury, J., Ferguson, T. A., & Caspi, R. R. (2012). The Rdb mutation of the Crb1 gene is present in vendor lines of C57BL/6N mice and embryonic stem cells, and confounds ocular induced mutant phenotypes. *Investigative Ophthalmology & Visual Science*, 53(6), 2921. <https://doi.org/10.1167/iovs.12-9662>
- McBee, J. K., Palczewski, K., Baehr, W., & Pepperberg, D. R. (2001). Confronting complexity: The interlink of phototransduction and retinoid metabolism in the vertebrate retina. *Progress in Retinal and Eye Research*, 20(4), 469–529. [https://doi.org/10.1016/S1350-9462\(01\)00002-7](https://doi.org/10.1016/S1350-9462(01)00002-7)
- Michael, H. T., Graff-Cherry, C., Chin, S., Rauck, C., Habtmichael, A. D., Bunda, P., ... Day, C.-P. (2018). Partial rescue of ocular pigment cells and structure by inducible ectopic expression of Mitf-M in MITF-deficient mice. *Investigative Ophthalmology & Visual Science*, 59(15), 6067. <https://doi.org/10.1167/iovs.18-25186>
- Mills, A. A., Zheng, B., Wang, X.-J., Vogel, H., Roop, D. R., & Bradley, A. (1999). p63 is a p53 homologue required for limb and epidermal morphogenesis. *Nature*, 398(6729), 708–713. <https://doi.org/10.1038/19531>
- Moore, B. A., Roux, M. J., Sebbag, L., Cooper, A., Edwards, S. G., Leonard, B. C., ... Moshiri, A. (2018). A population study of common ocular abnormalities in C57BL/6N rd8 Mice. *Investigative Ophthalmology & Visual Science*, 59(6), 2252. <https://doi.org/10.1167/iovs.17-23513>
- Muzumdar, M. D., Tasic, B., Miyamichi, K., Li, L., & Luo, L. (2007). A global double-fluorescent Cre reporter mouse. *Genesis*, 45(9), 593–605. <https://doi.org/10.1002/dvg.20335>
- Paterson, E. K., Fielder, T. J., MacGregor, G. R., Ito, S., Wakamatsu, K., Gillen, D. L., ... Ganesan, A. K. (2015). Tyrosinase depletion prevents the maturation of melanosomes in the mouse hair follicle. *PLoS ONE*, 10(11), e0143702. <https://doi.org/10.1371/journal.pone.0143702>
- Paterson, E. K., Ho, H., Kapadia, R., & Ganesan, A. K. (2013). 9-cis retinoic acid is the ALDH1A1 product that stimulates melanogenesis. *Experimental Dermatology*, 22, 202–209. <https://doi.org/10.1111/exd.12099>
- Phelep, A., Laouari, D., Bharti, K., Burtin, M., Tammaccaro, S., Garbay, S., ... Terzi, F. (2017). MITF – A controls branching morphogenesis and nephron endowment. *PLOS Genetics*, 13(12), e1007093. <https://doi.org/10.1371/journal.pgen.1007093>
- Pingault, V., Ente, D., Dastot-Le Moal, F., Goossens, M., Marlin, S., & Bondurand, N. (2010). Review and update of mutations causing Waardenburg syndrome. *Human Mutation*, 31(4), 391–406. <https://doi.org/10.1002/humu.21211>
- Pogenberg, V., Ögmundsdóttir, M. H., Bergsteinsdóttir, K., Schepsky, A., Phung, B., Deineko, V., ... Wilmanns, M. (2012). Restricted leucine zipper dimerization and specificity of DNA recognition of the melanocyte master regulator MITF. *Genes & Development*, 26(23), 2647–2658. <https://doi.org/10.1101/gad.198192.112>
- Reichrath, J., Münssinger, T., Kerber, A., Rochette-Egly, C., Chambon, P., Bahmer, F. A., & Baum, H. P. (1995). In situ detection of retinoid-X receptor expression in normal and psoriatic human skin. *The British Journal of Dermatology*, 133(2), 168–175. <https://doi.org/10.1111/j.1365-2133.1995.tb02612.x>
- Reinisalo, M., Putula, J., Mannermaa, E., Urtti, A., & Honkakoski, P. (2012). Regulation of the human tyrosinase gene in retinal pigment epithelium cells: The significance of transcription factor orthodenticle homeobox 2 and its polymorphic binding site. *Molecular Vision*, 18, 38–54.

- Robinson, J. T., Thorvaldsdóttir, H., Winckler, W., Guttman, M., Lander, E. S., Getz, G., & Mesirov, J. P. (2011). Integrative genomics viewer. *Nature Biotechnology*, 29(1), 24–26. <https://doi.org/10.1038/nbt.1754>
- Steingrímsson, E. (2008). All for one, one for all: Alternative promoters and Mitf. *Pigment Cell & Melanoma Research*, 21(4), 412–414. <https://doi.org/10.1111/j.1755-148X.2008.00473.x>
- Steingrímsson, E., Arnheiter, H., Hallsson, J. H., Lamoreux, M. L., Copeland, N. G., Jenkins, N. A., ... Shibahara, S. (2003). Interallelic complementation at the mouse Mitf locus. *Genetics*, 163(1), 267–276. <https://doi.org/10.1007/bf03023302>
- Steingrímsson, E., Copeland, N. G., & Jenkins, N. A. (2004). Melanocytes and the *Microphthalmia* transcription factor network. *Annual Review of Genetics*, 38(1), 365–411. <https://doi.org/10.1146/annurev.genet.38.072902.092717>
- Takeda, K., Hozumi, H., Nakai, K., Yoshizawa, M., Satoh, H., Yamamoto, H., & Shibahara, S. (2014). Insertion of long interspersed element-1 in the Mitf gene is associated with altered neurobehavior of the black-eyed white Mitfmi-bw mouse. *Genes to Cells*, 19(2), 126–140. <https://doi.org/10.1111/gtc.12117>
- Thorvaldsdóttir, H., Robinson, J. T., & Mesirov, J. P. (2013). Integrative genomics viewer (IGV): High-performance genomics data visualization and exploration. *Briefings in Bioinformatics*, 14(2), 178–192. <https://doi.org/10.1093/bib/bbs017>
- Trapnell, C., Pachter, L., & Salzberg, S. L. (2009). TopHat: Discovering splice junctions with RNA-Seq. *Bioinformatics*, 25(9), 1105–1111. <https://doi.org/10.1093/bioinformatics/btp120>
- Udono, T., Yasumoto, K. I., Takeda, K., Amae, S., Watanabe, K. I., Saito, H., ... Shibahara, S. (2000). Structural organization of the human microphthalmia-associated transcription factor gene containing four alternative promoters. *Biochimica Et Biophysica Acta-Gene Structure and Expression*, 1491, 205–219. [https://doi.org/10.1016/S0167-4781\(00\)00051-8](https://doi.org/10.1016/S0167-4781(00)00051-8)
- Vachtenheim, J., & Ondrusov, L. (2013). *MITF: A critical transcription factor in melanoma transcriptional regulatory network*. In Recent Advances in the Biology, Therapy and Management of Melanoma. InTech. <https://doi.org/10.5772/55191>
- Watanabe, K., Takeda, K., Yasumoto, K., Udono, T., Saito, H., Ikeda, K., ... Shibahara, S. (2002). Identification of a distal enhancer for the melanocyte-specific promoter of the MITF gene. *Pigment Cell Research*, 15(3), 201–211. <https://doi.org/10.1034/j.1600-0749.2002.01080.x>
- Wicks, N. L., Chan, J. W., Najera, J. A., Ciriello, J. M., & Oancea, E. (2011). UVA phototransduction drives early melanin synthesis in human melanocytes. *Current Biology: CB*, 21(22), 1906–1911. <https://doi.org/10.1016/j.cub.2011.09.047>
- Wildhardt, G., Zirn, B., Graul-Neumann, L. M., Wechtenbruch, J., Suckfüll, M., Buske, A., ... Steinberger, D. (2013). Spectrum of novel mutations found in Waardenburg syndrome types 1 and 2: Implications for molecular genetic diagnostics. *British Medical Journal Open*, 3(3), e001917. <https://doi.org/10.1136/bmjopen-2012-001917>
- Xie, X., Rigor, P., & Baldi, P. (2009). MotifMap: A human genome-wide map of candidate regulatory motif sites. *Bioinformatics*, 25(2), 167–174. <https://doi.org/10.1093/bioinformatics/btn605>
- Yajima, I., Sato, S., Kimura, T., Yasumoto, K.-I., Shibahara, S., Goding, C. R., & Yamamoto, H. (1999). An L1 element intronic insertion in the black-eyed white (Mitfmi-bw) gene: The loss of a single Mitf isoform responsible for the pigmentary defect and inner ear deafness. *Human Molecular Genetics*, 8(8), 1431–1441. <https://doi.org/10.1093/hmg/8.8.1431>
- Yang, A., Schweitzer, R., Sun, D., Kaghad, M., Walker, N., Bronson, R. T., ... McKeon, F. (1999). p63 is essential for regenerative proliferation in limb, craniofacial and epithelial development. *Nature*, 398(6729), 714–718. <https://doi.org/10.1038/19539>

SUPPORTING INFORMATION

Additional supporting information may be found online in the Supporting Information section at the end of the article.

How to cite this article: Flesher JL, Paterson-Coleman EK, Vasudeva P, et al. Delineating the role of MITF isoforms in pigmentation and tissue homeostasis. *Pigment Cell Melanoma Res.* 2020;33:279–292. <https://doi.org/10.1111/pcmr.12828>